

# Multiple Linear Regression Estimation of Onset Time Delay for Experimental Transcranial Narrowband Ultrasound Signals

Nathan Meulenbroek and Samuel Pichardo

**Abstract**—Focused Ultrasound is an emerging medical technique for transcranial procedures and requires the precise modelling of ultrasound signal propagation through the skull. To verify models, the onset time delay between two signals measured at the same spatial location, with and without the presence of a skull in the path of the signal, is compared between simulations and experiments. Current methods to automatically identify onset time delay use correlation-based algorithms. However, these techniques suffer from poor results caused by signal distortion and low signal-to-noise ratios in experimental signals. In this study, we compare the effectiveness of machine learning (multiple linear regression) to three correlation-based time delay estimation techniques in estimating the onset time delay of a signal pair. A sample of 1643 signal pairs, with center frequencies of either 270 kHz or 836 kHz, had their delays manually identified as a benchmark. Density, thickness, incidence angle, frequency, and x and y offsets from center were used as predictors. We find that, compared to manual identification, machine learning is 80.4% more accurate than cross-correlation across all test signals, and is noise-independent through all noise bins. The median of the errors were less than 0.3 periods was observed for signals with frequency 270 kHz, and less than 1.1 periods for signals with frequency 836 kHz, with little estimate bias. Overall, linear multivariable regression is determined to provide the best estimate of the onset time delay of two signals.

**Index Terms**—ultrasound, machine learning, cross-correlation, time delay.

## I. INTRODUCTION

**F**OCUSED Ultrasound (FUS) is a non-invasive treatment for various disorders that can concentrate mechanical energy on specific volumes within the body using high frequency sound waves. This energy can have various effects based on ultrasound parameters, such as intensity and frequency. For example, it can allow particle to cross through the blood-brain barrier [1], thermally ablate tissue [2], [3], or neurostimulate [4]. To achieve this, narrowband ultrasound pulses must be focused through the skull to a specific volume in the brain with high precision.

However, the tri-layer (cortical–diploë–cortical) composition of the skull can cause internal reverberations to form (both shear and longitudinal waves), resulting in positive or negative time delays in the measured onset of an ultrasound pulse [5]–[8]. This onset time delay (OTD), which is dependent on density, angle of incidence and other parameters, necessitates the

N. Meulenbroek is with the Departments of Physics and Astronomy and Computer Science, University of Calgary, Calgary, AB, T2N 1N4 Canada e-mail: nathan.meulenbroek@ucalgary.ca.

S. Pichardo is with the Departments of Radiology and Clinical Neurosciences, University of Calgary, Calgary, AB, T2N 1N4 Canada.

use of advanced propagation models to focus the ultrasound signals generated by a phased-array. Finite-difference time-domain (FDTD) models can predict the OTD of an arbitrary experimental setup, which is compared to the experimental OTD as a benchmark of accuracy [5], [6], [8], [9].

Cross-correlation, commonly used for time delay estimation [10]–[12], often misidentifies onset delay and require manual adjustment for the best results. Distortions and shifts in frequency associated with the interference of shear and longitudinal waves travelling through the skull violate the assumption that the two signals are similarly shaped, which is fundamental for cross-correlation. Regardless, due to their ubiquity and reliability in identifying time delay for the highest-amplitude section of a signal pair in medium to low noise situations, they have been used to inform manual identification in previous studies [9].

To eliminate the need for manual identification, we propose simple machine learning in the form of multivariable linear regression. Data available to us from Pichardo *et al.* [9] contains 59485 signal pairs, of which we have manually identified the delay for 1643 pairs. This subset is used for both training and testing, which we quantitatively compare to correlation-based methods.

An improved method for OTD is attractive for new studies where one of the signals in the calculation of the delay is highly distorted by the presence of an aberrator, such as in the case of transcranial ultrasound characterization. A robust, more reliable onset detection method is particularly of interest for the validation of new numerical methods aimed to improve the precision of simulated transcranial ultrasound [13]. In those types of studies, the simulated signal in the presence of a skull is also highly distorted. This problem is equally relevant when trying to align experimental or simulated signals in the time domain. Therefore validation with a more precise onset delay detection method will simplify the development of new numerical methods.

In this study, we analyze the effectiveness of three correlation-based algorithms and multivariable linear regression at identifying OTD relative to manual identification. To account for non-linear responses by the skull to the frequency of the ultrasound waves [8], results are grouped into two frequency bins with center frequency of 270 kHz and 836 kHz. Following this, due to various signal-to-noise ratios (SNRs), signals are further segmented into three approximately equal-size bins representing low, normal and high SNRs.

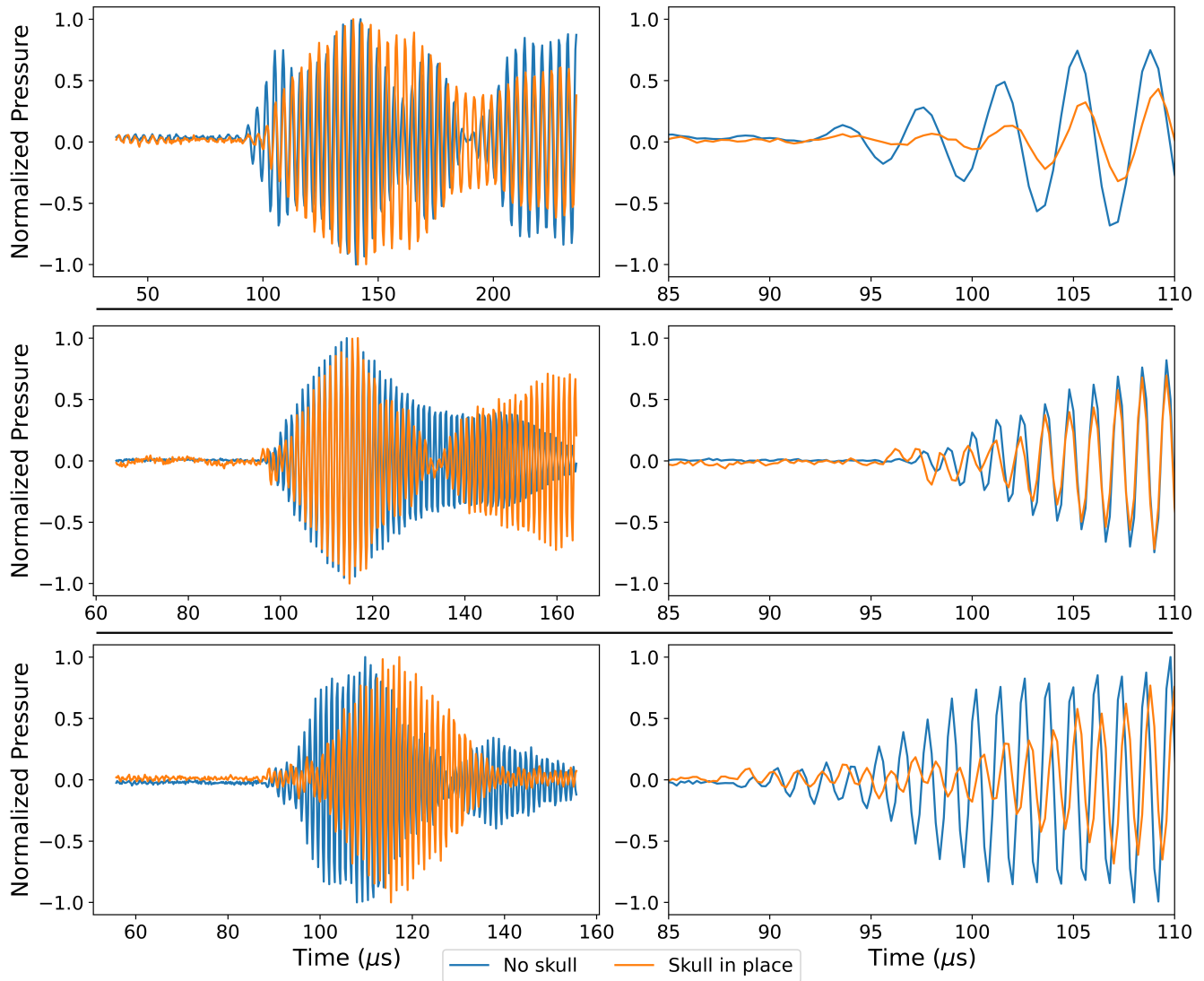


**Fig. 1. All:** Plots on the left are the full recorded signals, plots on the right are cropped to the onsets of the signals. Each of the above trials are on a different specimen. Signals were normalized such that the maximums and minimums of both signals were 1 and -1 respectively. **Top:** 270 kHz signal pair measured at an offset by ~5.08 mm right and ~14.61 mm up from center. **Middle:** 836 kHz signal pair measured at an offset of ~9.64 mm right and ~6.56 m up of center. **Bottom:** 836 kHz signal pair measured at an offset of ~11.49 m right and ~4.10 m up of center.

## II. METHODS

### A. Methodology

For this study, we randomly drew from a dataset of 59485 signal pairs, where each pair contained a signal recorded with a skull specimen between the detector and emitter (the aberrator signal), and a signal with only the detector and emitter (the water signal). Four specimens were included in the dataset, three of which are from Pichardo *et al.*'s 2017 dataset [9], and the fourth is from unpublished data but identically collected. Three different incident points were used on the two of the three published skulls, with the last using four. The unpublished specimen also used three.

Signals in a pair are matched by spatial location, such that the only difference is the presence of a skull specimen. A random sample of 1643 signals, selected using a uniform random distribution, was manually identified and used for training and analysis. Three examples of signal pairs in the

dataset are included in Fig. 1. OTD was then manually identified using a custom graphical user interface (GUI).

The SNR for a signal pair was taken as the ratio of the amplitude of the strongest sinusoid in the aberrator signal, as calculated by taking the maximum term from the Fourier Transform (excluding the DC term) (1), and the variance of the first 100 points in a signal. The first 100 points lie outside of the window where signals are generated, and so is taken to be white noise. Although there is noise present in both the aberrator and water signals, the SNR of the aberrator signal (2, where  $\sigma$  is standard deviation) was used to segment the signals since it was more often worse than the water signal's SNR.

$$\alpha(x) = \max(|\mathcal{F}(x)|) \quad (1)$$

$$\text{SNR} = \frac{\alpha(x_{\text{aberrator}})}{\sigma(x_{\text{aberrator}})} \quad (2)$$

TABLE I  
DATASET CHARACTERISTICS. THE DATASET INCLUDES DATA FROM FOUR SPECIMENS.

SNR	Full Dataset			Subset		
	270	836	Ratio	270	836	Ratio
High	2136	17693	0.12	97	452	0.21
Med.	2051	17777	0.12	100	447	0.22
Low	3782	16046	0.24	127	420	0.3
<b>Total</b>	<b>7969</b>	<b>51516</b>	<b>0.15</b>	<b>324</b>	<b>1319</b>	<b>0.25</b>

### B. Dataset

The signal data comes from thirteen target locations across four *ex-vivo* human skull specimens. It includes frequencies of 270 kHz and 836 kHz produced by an air backed transducer submerged in water. Interference within the air pocket caused a natural ramping, or slow onset, of the signal amplitude, reducing the SNR for the onset of the signals. The split of signals with frequencies of 270 and 836 kHz is summarized in Table I, which shows that the data has roughly similar ratios of frequencies for each SNR bin between the overall dataset and the subset. The sampling rate of the signals was either 2.5 samples/ $\mu$ s or 5 samples/ $\mu$ s for the frequencies of 270 kHz and 836 kHz, respectively.

For each specimen, a roughly circular grid of signal pairs was recorded, where each point in the grid was offset by half a wavelength of the emitted signal. The first signal in each pair was recorded without the skull in place and the second was recorded with the skull in place. The driving functions for the transducer in both scenarios were identical and therefore the only procedural difference was the presence of the skull. Pulse length was 15 ms and ramp-up and ramp-down effects were observed, although the ramp down in the skull signal was not identical to the water signal. The complete details regarding data acquisition, driving functions and experimental procedure can be consulted in Pichardo *et al.* 2017 [9].

The dataset we are using includes many features that were recorded at the time of the experiments. Only some are potentially useful for predicting onset time delay with many being descriptors with very little variation. Using correlation plots, we chose 6 features: density, thickness, angle of incidence, frequency, and x and y offset. These features are always accessible in *ex-vivo* contexts, for which this method is intended. All features, excluding density, were unmodified from the original dataset. Density was recorded at five different points surrounding the incident area. However, the individual measurements were highly correlated to each other. We therefore substituted the average of these five points. We also trained the model with more features, though we found this resulted in over-fitting. Therefore, we chose the best performing set of features.

### C. Manual Identification of Time Delay

Onset time delay for the set of 1643 signal pairs was manually identified by three individuals using a custom GUI (pictured in Fig. 2), which allowed the user to drag the aberrated signal across the water signal in real time. A slider

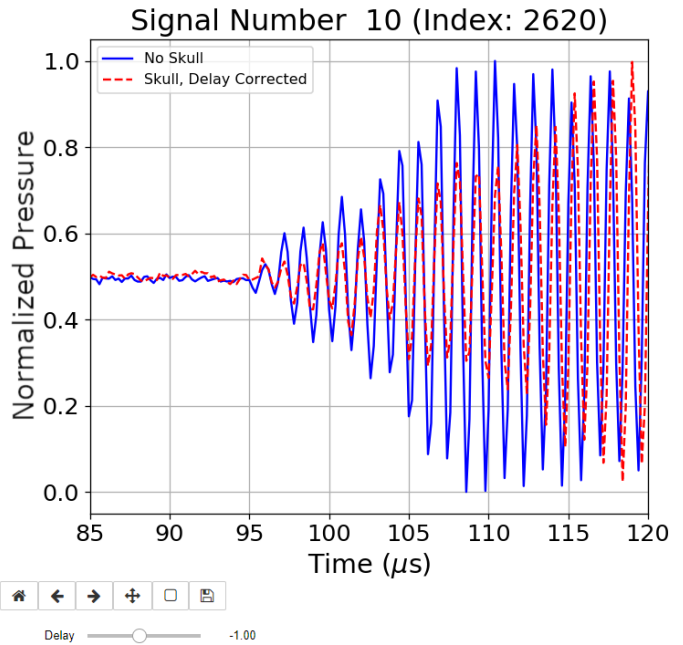


Fig. 2. The graphical user interface (GUI) used to manually identify OTD. Made using Python Jupyter Widgets. The slider at the bottom of the graph can be dragged to vary the positioning of the red signal in real time. OTD for this signal has been determined to be -1.00 seconds due to the first few oscillations of both the red and blue signals matching up visually identically.

allowed the user to move the aberrated signal in increments of 0.02  $\mu$ s, which appeared smooth to the human eye. The onset delay for a signal pair was said to be correctly identified when the first visible oscillation of both signals were aligned, disregarding oscillations which come afterwards, as depicted in Fig. 2. To verify that there was no estimation bias unique to an individual user, 90 random signal pairs were analyzed independently by all the readers, and statistical tests were performed to establish if there was or no a reader bias.

### D. Time Delay Estimators

Time delay estimators are required for many different forms of signal processing, and there are a variety of techniques available [14]–[17]. Several variations of correlation-based algorithms are commonly used in the field, from which we chose three to use as benchmarks. Cross-correlation, without filters or interpolation, was chosen for its simplicity and reliability for similarly shaped signals. We also chose two variants which use filters borrowed from the field of onset detection [18], [19]. The first variant reduces the input signal to its spectral energy over time, tuned to look for signals of a specified frequency. The second variant reduces the signal to its envelope using the Hilbert transform.

1) *Spectral Energy*: By finding the energy (3) of the short time Fourier transform (STFT), the onset of a sinusoid at the desired frequency appears as a rising edge. For 270 kHz signals, the sampling rate is 2.5 samples/ $\mu$ s and thus the Nyquist frequency is 1250 kHz. Similarly, the sampling rate at 836 kHz is 5 samples/ $\mu$ s and the Nyquist frequency is 2500 kHz. We determined the size of the buffer by dividing the sampling rate by the frequency. Since we expect distortions

to vary the frequency of the signal received, a margin of 50% was added to the size of the buffer (4). Buffers are overlapped to retain input resolution. Points without a full buffer available are discarded. A Hann window is used to minimize spectral leakage. The spectral energy of both signals are used as inputs for a simple cross-correlation algorithm.

$$E(x) = \sum_{n=0}^N x[n] \cdot \bar{x}[n] \quad (3)$$

$$\text{Buffer Size} = \frac{\text{Sampling Rate}}{\text{Frequency}} * 1.5 \quad (4)$$

$$\text{Hann Window}(n) = 0.5(1 - \cos(2\pi n)) \quad (5)$$

2) *Hilbert Transform*: The second variation uses the Hilbert transform to convert the waveform to an envelope. In the time domain, the transform is evaluated by the convolution in Equation (6), where  $f(t)$  is the input function over time. The result is the original signal with a phase shift of  $-\pi/2$  for all frequencies. The envelope of the signal is the magnitude of the original signal as the real component and the Hilbert transform as the imaginary component (7). The envelope for both signals in a pair is then used as input for cross-correlation to find the onset delay.

$$\mathcal{H}(t) = \left( \frac{1}{\pi t} \right) * f(t) \quad (6)$$

$$A(t) = |f(t) + i\mathcal{H}(t)| \quad (7)$$

### E. Multivariable Linear Regression

Multivariable linear regression was identified as an adequate machine learning approach for this case based on literature claims that many of the features which we are using are linearly related to onset delay [8], [20], [21]. We took a uniform random sample of 70% of the dataset, 1150 signal pairs, as the training set and the remaining 30%, or 493 signals, were used as our test set. The regression fit was determined by minimizing the residual on the training set using the normal equation. We used six features in total, listed in Table II.

We used the normal equation (8, where  $X$  is the design matrix and  $y$  is a vector of manually identified delays corresponding to  $X$ ) since it will run in a reasonable amount of time with the size of our dataset and it doesn't require the manual selection of parameters. We used the regularized equation, with regularization parameter  $\lambda$ , to guarantee the invertibility of the matrix. We did not see significant improvements when varying the regularization parameter, and it was therefore left as 1.

$$\Theta = \left( X^T X + \lambda \begin{bmatrix} 0 & 0 & 0 & \dots & 0 \\ 0 & 1 & 0 & \dots & 0 \\ 0 & 0 & 1 & \dots & 0 \\ \dots & \dots & \dots & \dots & \dots \\ 0 & 0 & 0 & \dots & 1 \end{bmatrix} \right)^{-1} X^T y \quad (8)$$

Multivariable polynomial regression was also considered to address underfitting in initial tests with a smaller dataset. The X and Y offsets were fit with a polynomial since it is not known if they are linearly related to delay, and there were not enough datapoints to justify a nonlinear fit with respect to

TABLE II  
LIST OF FEATURES EXTRACTED FROM DATASET.

Feature	Description
Density	Average density of skull (Kg/m <sup>3</sup> )
Thickness	Average thickness of skull at impact site (cm)
Incidence angle	Angle of wave relative to skull surface normal (°)
Frequency	Frequency of ultrasound signal (kHz)
X offset	X coordinate relative to center (# Periods)
Y offset	Y coordinate relative to center (# Periods)

frequency. We used a sample of 60% for the training set, 20% for the test set, and 20% as a cross-validation set for multiple degree polynomials, but did not see a significant improvement with increased degrees.

### F. Sensitivity Analysis

To analyse which of the features were most pertinent for OTD estimation, we used standardized regression coefficients. This scales the individual coefficients such that one standard deviation of change in a feature will produce the computed fraction of the standard deviation of the overall results in a result. Normalized coefficients are computed using Equation (9), where  $x_i$  is the coefficient corresponding to feature  $i$ ,  $\sigma_x$  is the standard deviation of that feature, and  $\sigma_y$  is the standard deviation of the results.

$$x_{i,\text{norm}} = x_i \frac{\sigma_x}{\sigma_y}, \quad (9)$$

### G. Statistics

To quantify the error of the different methods in relation to manually identified delay, we used the absolute median difference (10). To quantify the bias of the different methods in relation to manually identified delay, we used the median difference (11). Neither the distributions of the absolute differences or the differences were normal and the median was used instead of the mean. However, they were similar both between algorithms and SNR bins and therefore a two-sided Mann-Whitney U test was used to test for significance.

$$\text{Abs. Median Diff.}(x, y) = \text{median}(|x - y|) \quad (10)$$

$$\text{Median Diff.}(x, y) = \text{median}(x - y) \quad (11)$$

### H. Evaluating Accuracy

The characterization of transcranial FUS often uses Cartesian grid sampling to identify areas of high acoustic pressure within a volume. For this reason, OTD estimates can draw from the context of the surrounding points to help in the identification of estimates which exceed a certain error threshold or are not consistent with their surroundings. Therefore, the expectations for the accuracy of this algorithm need not be as stringent as for single measurement applications. Given that points in a grid are half a wavelength apart, a tolerance of half a period in either direction is acceptable for our use case. Error lower than half a period aligns peaks sufficiently in the context of a grid to allow the comparison of estimated experimental OTDs to simulated OTDs.

TABLE III  
CHARACTERISTICS OF SNR SEGMENTATION BINS.

SNR bin	Lowest SNR in bin (dB)	Mean (dB)	Highest SNR in bin (dB)	Bin Size
Combined				
High	10.37	13.77	17.17	165
Med.	7.19	8.77	10.36	164
Low	-2.56	2.31	7.19	164
270 kHz				
High	10.73	13.95	17.17	36
Med.	6.59	8.57	10.55	34
Low	-2.56	2.01	6.58	34
836 kHz				
High	10.33	13.52	16.71	131
Med.	7.44	8.87	10.29	129
Low	1.03	4.21	7.39	129

TABLE IV  
STANDARDIZED COEFFICIENTS FOR EACH FEATURE.

Feature	Standardized Coefficient
Density	-0.5115
Thickness	-0.1079
Incidence angle	-0.5757
Frequency	-0.8977
X offset	0.8056
Y offset	0.1074

The coefficients above correspond to the fraction of the standard deviation of the result (where the result is the OTD estimate) a change of one standard deviation in each of the features would produce. Normalized coefficients are directly comparable with each other, but not with other models.

### III. RESULTS

Table III shows a summary of the SNR classification of the signals in the test set ( $n = 493$ , 30% of the dataset). Table IV shows the standardized regression coefficients. Notably, the features which influence OTD estimates the most are frequency and X offset, and Y offset and thickness influence estimates the least.

Fig. 3 summarizes the error and estimation bias for the three correlation methods and multivariable regression in units of microseconds for both frequencies. From the top plot, it is clear that the machine learning technique demonstrates strongly significantly lower absolute median difference in all bins ( $p < 0.0001$ ). The absolute median difference of the linear multivariable regression technique is also 80.4% more accurate than the cross-correlation method, and its interquartile range is 77.8% smaller. All of the correlation methods show a bias towards underestimating the true OTD, to be contrasted with multivariable regression which is more closely zero centered.

Fig. 4 segments the results into frequency bins. On the left is the error (top) and bias (bottom) for 270 kHz, and similarly on the right for 836 kHz. Units for these plots are expressed in periods, which helps establish the performance of the algorithms relative to the frequency of the signals. Again, it is clear that multivariable regression is best overall. Significance is not as strong for the 270 kHz signals as it is for the 836 kHz signals. A contributing factor to this may be that there are fewer 270 kHz datapoints in the dataset. The overall

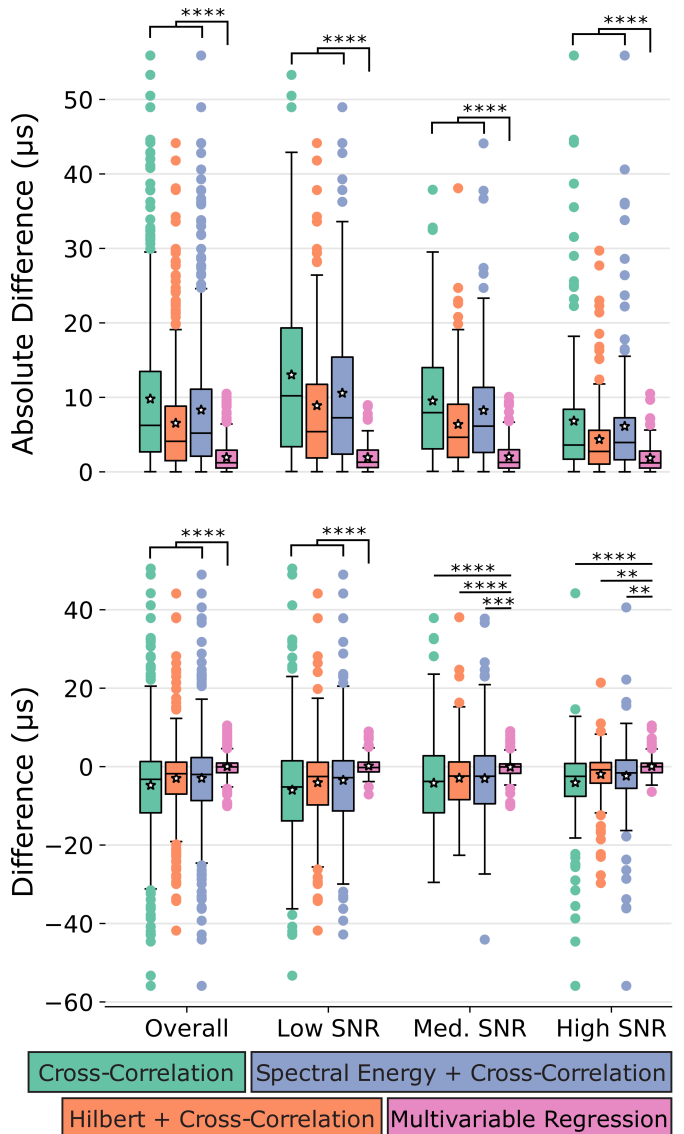
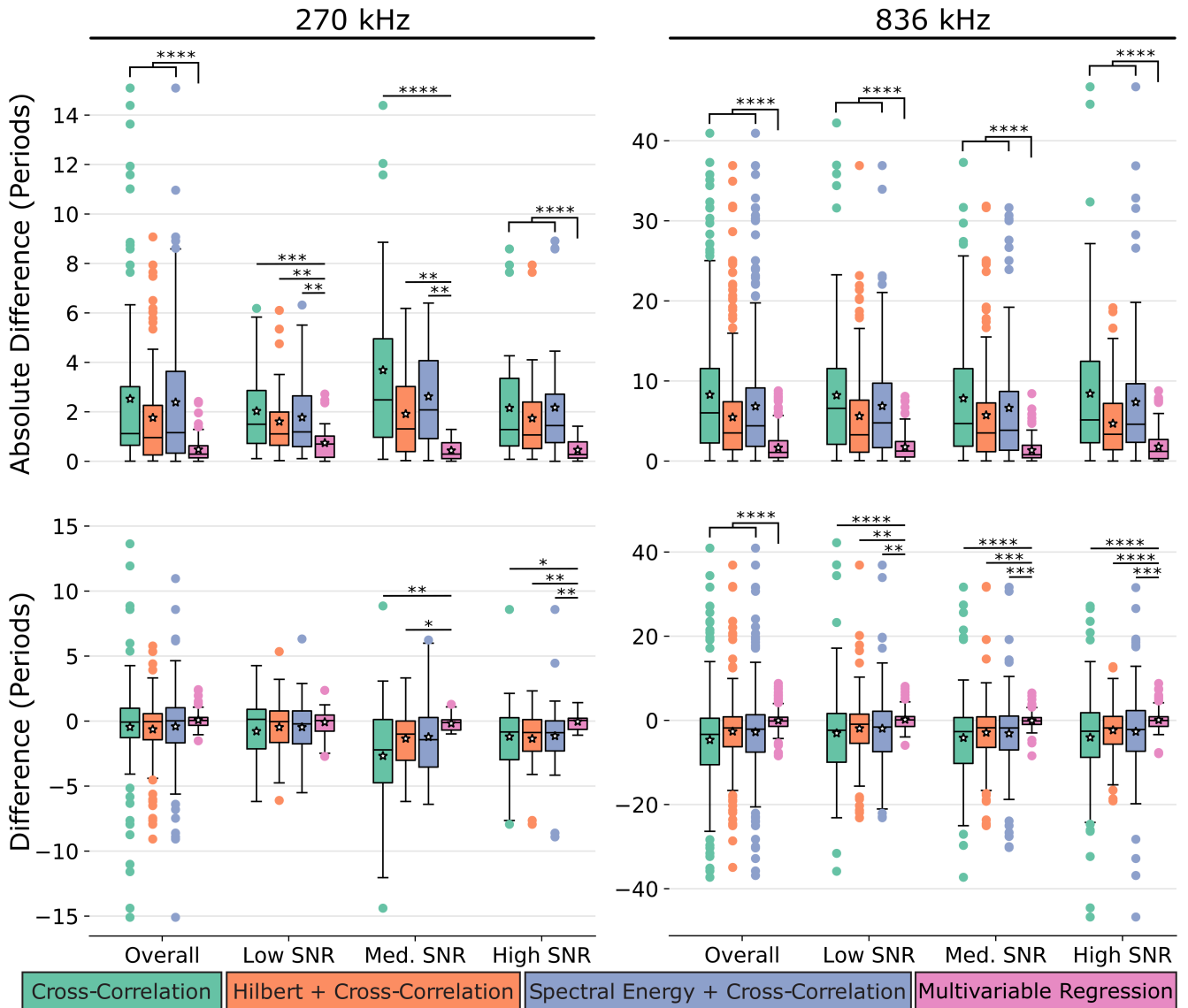


Fig. 3. **Top:** Error of each algorithm relative to the manually identified onset time delay. **Bottom:** Bias of each algorithm relative to manual identification. **Both:** Averages indicated by white stars. \*\* significant at  $p < 0.01$ , \*\*\* significant at  $p < 0.001$ , \*\*\*\* significant at  $p < 0.0001$  (Mann-Whitney U Test).

error for 270 kHz signals is approximately 0.29 periods, and 1.08 periods for 836 kHz signals. Error of less than 0.5 periods was also achieved for both the medium and high SNR 270 kHz signals (0.29 and 0.27 periods respectively). Multivariable regression also outperforms the correlation-based methods in terms of bias as well. The correlation methods show a (quite often significantly) stronger bias towards under-estimating the delay than multivariable regression.

All of the algorithms perform comparatively worse in the 836 kHz case than in the 270 kHz case. A significance test between frequencies was not conducted since one period at 836 kHz is smaller than that at 270 kHz. There is no significant difference between any error or bias noise bins for either the 270 kHz case or the overall case when using multivariable regression, where the smallest  $p$ -value is  $p = 0.12$ . There is significance between the low and medium SNR error bins in



**Fig. 4.** **Left:** Error and bias of each algorithm for signals with frequency of 270 kHz. **Right:** Error and bias of each algorithm for signals with frequency of 836 kHz. **Both:** Note that the difference is now measured in periods. Averages indicated by white stars. \* significant at  $p < 0.05$ , \*\* significant at  $p < 0.01$ , \*\*\* significant at  $p < 0.001$ , \*\*\*\* significant at  $p < 0.0001$  (Mann-Whitney U Test).

the 836 KHz case ( $p = 0.03$ ), but not between the low and high SNR and medium and high SNR error bins ( $p = 0.74$  and  $p = 0.10$  respectively) or any of the bias bins.

The distribution of the 90 delays analyzed among all readers was similar, but not Gaussian. Therefore, a Mann-Whitney U test was used to confirm that the difference between the means was not significant ( $p = 0.15$ ).

#### IV. DISCUSSION

Overall, machine learning for onset delay estimation seems promising when compared to correlation-based methods. The median difference for all variants is very strongly significantly lower than the correlation benchmarks in most cases, with the exception of the 270 kHz signals, which have fewer signal pairs in our dataset. We are therefore confident that machine learning is a better estimator in all proposed situations.

However, the median differences hides some of the subtleties of how the different algorithms perform. In low noise scenarios, we anecdotally noticed that machine learning was not able to reach the exact solution as identified by both the correlation methods and manual identification. This may suggest that small, manual refinements of the multivariable regression estimate are required for a perfect solution.

It is also interesting to note that the performance of cross-correlation with the Hilbert transform filter exceeds that of cross correlation alone. This suggests that when identifying the onset of a signal, phase information (which is removed by the filter) is not important for onset detection. The filter may also help to minimize peak-hopping errors introduced by cross-correlation.

The standardized coefficients in Table IV also provide some context as to which features are most important for estimation of OTD. The importance of x position (left/right within a spec-

imen) is more important than y position (anterior/posterior), which implies stronger curvature or change in bone structure left/right than anterior/posterior. The results also show that the thickness of the skull at the incident point does not influence the results as much as other features. Since our dataset only includes four specimens, however, biases in our dataset may influence the apparent bias in the standardized coefficients. For this reason, more specimens may be required before these results are generalizable.

The non-significant difference between multivariable regression noise bins, even considering the one 836 KHz exception, makes the method attractive to use with low SNR signals in particular, which can be difficult to identify by the human eye. Notably, it performs with sufficient accuracy and precision to independently identify OTD in medium and high SNR 270 kHz signals, since it reaches below the 0.5 period threshold required to properly focus sound waves. Regardless, we do not yet recommend the complete replacement of manual identification as there is still room for improvement in other cases.

One key advantage of multivariable regression over the correlation methods is its ability to estimate error in a more zero-centered fashion. When we observe positive OTD, or the aberrator signal is delayed, this means that shear waves dominate since the signal is slowed [9]. Similarly, when the OTD is negative, this tells us that longitudinal waves are dominating because the signal has crossed a path with the same length in a shorter time. When using a correlation algorithm, if the delay is consistently underestimated, we may misinterpret this to mean that longitudinal waves are dominating when, in fact, shear waves dominate.

An important consideration in our study is the use of narrowband signals with a large number of pulses. When narrowband signals cross the skull, the resulting frequency distortions make it especially challenging to match aberrator signals with water-only signals. This distortion can contribute to why methods such as cross-correlation demonstrate poor performance. The proposed method in this study aims to address this problem. Narrowband signals are highly relevant for numerical studies as it minimizes memory and processing costs when techniques can be optimized for a central frequency. The use of broadband pulses, while potentially simplifying the delay estimation, demands using numerical conditions capable to handle the highest frequency in the signal, increasing significantly computational costs, which may be unnecessary for studies aiming to characterize therapeutic applications that utilize narrowband conditions.

#### A. Study Limitations

Cross-correlation, when applied to an application such as this, will be inherently biased towards the more intense part of the signal. Due to peak-hopping effects and background noise, cross-correlating is further hampered when aligning the smallest peaks of a signal pair. The two filters employed help to mitigate the effects of noise, though cross-correlation is still biased towards the bulk of the signal.

More variability in frequency and density, which are limited because of physical limitations to transducers and the number

of specimens available at any one time, may help to improve results. Experiments at more frequencies might reveal a more complex relationship between OTD and frequency. Additional variability in density would further increase our confidence in the generality of these results, which we know from previous studies to be correlated with OTD. We would also like to explore the addition of new features through new density analysis techniques, such that we can better account for the effect of internal reflection within the skull.

We also found that the ratios of signal bins in Table I, although similar to the overall dataset, were not exactly the same. A new random sample or more frequencies from other experiments could address the 270 KHz signals performing better in terms of periods than 836 KHz. However, given the majority of signals in the subset are 836 KHz signals as it stands, we expect improvements from implementing these changes to be marginal.

## V. CONCLUSION

Overall, multivariable linear regression was shown to be 80.4% more accurate than cross-correlation in estimating OTD. Machine learning also demonstrated a lack of dependence on noise and significantly less bias than correlation-based methods. It was also shown that correlation-based methods tend to underestimate OTD, which could lead to misinterpretation of the results. Although multivariable regression has shown large improvements over its predecessors, it has only met the goal of 0.5 periods error for 270 kHz signals. Therefore, we continue to recommend small manual adjustments for the identification of onset time delay.

## ACKNOWLEDGMENT

The authors would like to thank Nils Forkert for insightful comments that helped us start this effort, Jacqueline Seal and William Wynne for their assistance with manually identifying onset delay in the dataset, and Paula Brandt for her relentless proofreading. The authors would also like to thank the Natural Sciences and Engineering Research Council of Canada Discovery Grant for their financial support.

## REFERENCES

- [1] L. H. Treat, N. McDannold, N. Vykhotseva, Y. Zhang, K. Tam, and K. Hyynnen, "Targeted delivery of doxorubicin to the rat brain at therapeutic levels using MRI-guided focused ultrasound," *Int. J. Cancer*, vol. 121, no. 4, aug 2007. [Online]. Available: <http://doi.wiley.com/10.1002/ijc.22732>
- [2] N. McDannold, G. T. Clement, P. Black, F. Jolesz, and K. Hyynnen, "Transcranial magnetic resonance imaging-guided focused ultrasound surgery of brain tumors: initial findings in 3 patients," *Neurosurgery*, vol. 66, no. 2, pp. 323–332, 2010.
- [3] W. J. Elias, D. Huss, T. Voss, J. Loomba, M. Khaled, E. Zadicario, R. C. Fryssinger, S. A. Sperling, S. Wylie, S. J. Monteith *et al.*, "A pilot study of focused ultrasound thalamotomy for essential tremor," *New England Journal of Medicine*, vol. 369, no. 7, pp. 640–648, 2013.
- [4] W. Legon, T. F. Sato, A. Opitz, J. Mueller, A. Barbour, A. Williams, and W. J. Tyler, "Transcranial focused ultrasound modulates the activity of primary somatosensory cortex in humans," *Nature neuroscience*, vol. 17, no. 2, pp. 322–329, 2014.
- [5] C. W. Connor, G. T. Clement, and K. Hyynnen, "A unified model for the speed of sound in cranial bone based on genetic algorithm optimization," *Phys Med Biol*, vol. 47, no. 22, pp. 3925–3944, 2002.

- [6] J. F. Aubry, M. Tanter, M. Pernot, J. L. Thomas, and M. Fink, "Experimental demonstration of noninvasive transskull adaptive focusing based on prior computed tomography scans," *J Acoust Soc Am*, vol. 113, no. 1, pp. 84–93, 2003.
- [7] G. T. Clement, P. J. White, and K. Hyynnen, "Enhanced ultrasound transmission through the human skull using shear mode conversion," *J Acoust Soc Am*, vol. 115, no. 3, pp. 1356–1364, 2004.
- [8] S. Pichardo, V. W. Sin, and K. Hyynnen, "Multi-frequency characterization of the speed of sound and attenuation coefficient for longitudinal transmission of freshly excised human skulls," *Phys. Med. Biol.*, vol. 56, no. 1, jan 2011. [Online]. Available: <http://www.ncbi.nlm.nih.gov/pubmed/21149950> <http://www.ncbi.nlm.nih.gov/article/PMC3166773>
- [9] S. Pichardo, C. Moreno-Hernández, R. Andrew Drainville, V. Sin, L. Curiel, and K. Hyynnen, "A viscoelastic model for the prediction of transcranial ultrasound propagation: application for the estimation of shear acoustic properties in the human skull," *Phys. Med. Biol.*, vol. 62, no. 17, aug 2017. [Online]. Available: <http://www.ncbi.nlm.nih.gov/pubmed/28783716> <http://www.ncbi.nlm.nih.gov/article/PMC5751709>
- [10] F. Viola and W. F. Walker, "A comparison of the performance of time-delay estimators in medical ultrasound," *IEEE T Ultrason. Ferr.*, vol. 50, no. 4, pp. 392–401, apr 2003. [Online]. Available: <http://www.ncbi.nlm.nih.gov/pubmed/12744395>
- [11] S. Bjorklund and Lennart Ljung, "A review of time-delay estimation techniques," in *42nd IEEE International Conference on Decision and Control (IEEE Cat. No.03CH37475)*, vol. 3. IEEE, 2003. [Online]. Available: <http://ieeexplore.ieee.org/document/1272997/>
- [12] A. K. Nandi, "On the subsample time delay estimation of narrowband ultrasonic echoes," *IEEE T. Ultrason. Ferr.*, vol. 42, no. 6, nov 1995. [Online]. Available: <http://ieeexplore.ieee.org/document/476542/>
- [13] R. A. Drainville, L. Curiel, and S. Pichardo, "Superposition method for modelling boundaries between media in viscoelastic finite difference time domain simulations," *The Journal of the Acoustical Society of America*, vol. 146, no. 6, pp. 4382–4401, 2019.
- [14] F. Viola and W. F. Walker, "A spline-based algorithm for continuous time-delay estimation using sampled data," *IEEE Transactions on Ultrasonics, Ferroelectrics, and Frequency Control*, vol. 52, no. 1, pp. 80–93, jan 2005.
- [15] S. Langeland, J. D'hooge, H. Torp, B. Bijnens, and P. Suetens, "A simulation study on the performance of different estimators for two-dimensional velocity estimation," in *Proceedings of the IEEE Ultrasonics Symposium*, vol. 2, 2002, pp. 1859–1862.
- [16] A. Fertner and A. Sjolund, "Comparison of Various Time Delay Estimation Methods by Computer Simulation," *IEEE Transactions on Acoustics, Speech, and Signal Processing*, vol. 34, no. 5, pp. 1329–1330, 1986.
- [17] G. Jacobitti and G. Scarano, "Discrete Time Techniques for Time Delay Estimation," *IEEE Transactions on Signal Processing*, vol. 41, no. 2, pp. 525–533, 1993.
- [18] J. C. Glover, "Sinusoids, noise and transients: spectral analysis, feature detection and real-time transformations of audio signals for musical applications," *IR eTheses*, 2012, (PhD Thesis). [Online]. Available: <http://eprints.maynoothuniversity.ie/4523/>
- [19] J. Bello, L. Daudet, S. Abdallah, C. Duxbury, M. Davies, and M. Sandler, "A tutorial on onset detection in music signals," *IEEE T. Speech Audi. P.*, vol. 13, no. 5, pp. 1035–1047, sep 2005. [Online]. Available: <http://ieeexplore.ieee.org/document/1495485/>
- [20] P. J. White, G. T. Clement, and K. Hyynnen, "Longitudinal and shear mode ultrasound propagation in human skull bone," *Ultrasound Med. Biol.*, vol. 32, no. 7, pp. 1085–96, jul 2006. [Online]. Available: <http://www.ncbi.nlm.nih.gov/pubmed/16829322> <http://www.ncbi.nlm.nih.gov/article/PMC1560344>
- [21] T. D. Webb, S. A. Leung, J. Rosenberg, P. Ghanouni, J. J. Dahl, N. J. Pelc, and K. B. Pauly, "Measurements of the Relationship Between CT Hounsfield Units and Acoustic Velocity and How It Changes With Photon Energy and Reconstruction Method," *IEEE T. Ultrason. Ferr.*, vol. 65, no. 7, pp. 1111–1124, jul 2018. [Online]. Available: <https://ieeexplore.ieee.org/document/8340162/>



**Nathan Meulenbroek** received his bachelor degrees in Computer Science and Physics from the University of Calgary in 2020. He will be commencing his graduate work in Biomedical Engineering the same year. Nathan has been a part of the NeuroFUs Lab at the University of Calgary as a student researcher since 2018.



**Samuel Pichardo** obtained his Ph.D. in Imaging and Systems in 2005 from the INSA-Lyon, France, while conducting his research at the INSERM LabTau laboratory. From 2006 to 2008, he worked as a Postdoctoral fellow at Sunnybrook Research Institute and from 2008 to 2017, Samuel worked as scientist in the Thunder Bay Regional Health Research Institute and was an adjunct professor at Lakehead University. He joined the University of Calgary in 2017 as assistant professor in the Departments of Radiology and Clinical Neurosciences, Cumming School of Medicine, and as a member of the Hotchkiss Brain Institute.